Investigation of thin-film CIGS degradation under P2 scribe laser illumination

Kamil Stelmaszczyk[1,2,*], Christof Schultz[1], Manuel Schüle[1], Moshe Weizman[1], Christian A. Kaufmann[2], Rutger Schlatmann[1,2], Björn Rau[2], Volker Quaschning[1], Bert Stegemann[1], and Frank Fink[1]

[1]*PVcomB/ HTW Berlin - University of Applied Sciences, Wilhelminenhofstr. 75a, D-12459 Berlin*
[2]*PVcomB/ Helmholtz-Zentrum Berlin für Materialien und Energie GmbH, Schwarzschildstr. 3, D-12489 Berlin*

*Corresponding author:
kamil.stelmaszczyk@htw-berlin.de, Phone: +49 30 5019 3529

Abstract: We present a study of the degradation of thin-film CIGS material in the vicinity of P2 phase-transformation type of laser scribes. They comprised optical microscopy, scanning electron microscopy, energy dispersive X-ray spectroscopy, photoluminescence and Raman spectroscopy. While the optical and electron microscopy measurements have shown a clear change of the morphological properties of CIGS including removal, melting and dislocation of material from the area scribed by the laser, the X-ray analysis revealed an accumulation of O, Zn, Ga, and Cu elements in the melted phase and an evaporation of more volatile In atoms from the region of visually changed CIGS. At the same time Raman and photoluminescence measurements have shown substantial alteration of semiconductor material properties, i.e. of the crystallinity and the bandgap energy even far beyond of this region. More precisely, the amplitudes of the A_1 and B_2,E Raman peaks were found to increase continuously with increasing distance from the P2 scribes, reaching the distances of approximately three times the 3σ diameter of the beam. A similar tendency was also observed for photoluminescence signals, that additionally revealed a systematic shift of the bandgap energy in CIGS as estimated from the maximum of the emission spectrum. Our results indicate that the phase-transformation scribing generates changes in thin-film CIGS material far beyond the heat affected zone. As such they can help to decide on optimal spacing between P1-P3 scribes and thus reduce a "dead area" of thin-film CIGS solar cells.

1 Introduction

Laser processing of thin-film solar cells attracts attention due to its practical implementations in industrial production lines [1]. Their most important advantage over classical processing is the elimination of mechanical scribing which is known to introduce damage over a large area near the scribe due to clipping and chipping caused by a contact with mechanical tip [2]. Laser scribing can be applied on each of production of thin-film $Cu(In_x,Ga_{1-x})Se_2$ (CIGS) solar cells. The three types of processes are defined in this case including the so called P1, P2 and P3 scribes [3,4]. The P1 scribes are made to ablate narrow molybdenum (Mo) stripes from the freshly prepared glass substrates. Their role is to isolate the areas on which individual solar cells will be fabricated. The second type of scribes - the P2 scribes - is needed to achieve current flow between adjacent solar cells and connect the back contact Mo layer with a front contact, typically made of a transparent conductive oxide (TCO). They are usually applied after a deposition of the absorber material and before sputtering of TCO. The final P3 scribes serve to remove either the TCO or the TCO and absorber layers simultaneously. Since a distance from P3 to P1 scribes defines an active area of a cell, their positions must be carefully chosen. On the other hand, the spacing between P1 and P2 scribes and between P2 and P3 determines the size of the so called "dead area" of the cell, which should be as small as possible for an effective usage of a photoactive area. This explains the importance of careful adjustment of P1 and P3 positions for obtaining best performing solar cells. While successful P1-P3 scribing applying short ps laser pulses has been demonstrated [5,6], mechanical needles are still preferred for P2 scribing in industrial fabrication [7]. However, both techniques are similar from the production sequence point of view, as they must be applied before deposition of the TCO. Such approach demands extensive handling because the P2 and P3 scribes are made in two successive but independent scribing steps. This is why a new concept of performing P2 pattering has been proposed recently which exploits the idea of thermal decomposition of CIGS through the TCO barrier by means of ns laser radiation [8,9]. Providing sufficiently long interaction time between a laser pulse and the matter, the initially non-conducting CIGS can be transformed into conducting material containing enhanced quantities of liberated metallic compounds [10,11]. These are these compounds that conduct the current through the P2 scribes. Although much of the attention has been paid to the electrical properties of phase transformed P2 scribes [11,12], almost no information can be found on the defects that might be created in the semiconductor material. This is rather surprising since as a heat sensitive material CIGS is known to decompose at about 500 °C [13], i.e. at a temperature which can be easily achieved during laser ablation. In this paper we show how the P2 type phase transformation scribes might degrade the CIGS and cause a limited performance. The influence of the scribing laser beam energy on the physical and chemical properties of CIGS like morphology, crystalline state, chemical composition or a bandgap structure was investigated Consequently, we have used several experimental

techniques to characterize the laser effect starting from Optical Microscopy (OM), Scanning Electron Microscopy (SEM) or Energy Dispersive X-Ray Spectroscopy (EDX) to Photoluminescence (PL) and Raman (RA) Spectroscopy. The energy of P2 pulses covered a wide range of process window estimated in a separate experiment in which the series resistance of cells, R_s, was measured as a function of the laser pulse energy. Basing on a set of measured current-voltage (I-V) characteristics of solar cells the minimum of R_s=4.5 $\Omega \cdot cm^2$ was found corresponding to a laser pulse energy of 4.47 µJ. Details about this experiment can be found in [12].

2 Experimental approach

2.1 CIGS Samples

The baseline process of the Competence Center for Thin-Film and Nanotechnology for Photovoltaics in Berlin (PVcomB), following a sequential growth of functional cell layers was used for manufacturing of CIGS samples [14]. After cleaning, the soda lime glass (SLG) is transferred into the in-line magnetron tool (Leybold Optics A600V) for sputtering of the SiO_xN_y barrier and the back contact Mo layer. The Mo is next scribed in the P1 type of process using an integrated laser patterning facility (Rofin Baasel Lasertech). The pattering is made at 1064 nm wavelength and with a ps laser source (Time Bandwidth, Duetto). In the subsequent step, the precursor absorber layer of copper (Cu), gallium (Ga) and indium (In) is sputtered. The probe is selenized (Se) and annealed in a rapid thermal furnace (Centrotherm). In a next step, the buffer CdS is deposited by a wet chemical process and the front contact Transparent Conducting Oxide (TCO) layer comprising i-ZnO and ZnO:Al is sputtered in the VIS300 tool (Ardenne Anlagentechnik). The CIGS stacks are once again processed by the ps laser in the final P3 scribe. The samples produced in the above process consist of 1 µm thick TCO layer (including 150 nm i-ZnO), 40-50 nm CdS buffer layer, 1.6 µm thick absorber layer (CIGS) and 850 nm thick back contact Mo layer with ~150 nm SiO_xN_y barrier. Such complete solar cell stacks were next processed by the phase transformation P2 scribes.

2.2 P2 Phase Transformation Scribing

For the P2 patterning, CIGS samples are positioned on the x-y translation stage (Aerotech). This linear-motor driven unit has the pre-selectable working velocities of up to 1.2 m s^{-1}. A nominal reproducibility of position is 5 µm for each of the axes, however, for the purpose of the experiment the samples were moved along one axis, forming individual vertical lines separated by a fixed distance of 250 µm. Their pattern on the substrate is shown in the Figure 1a. The Q-switched, diode-pumped ns laser (SL 3 SHG PV, Rofin Baasel Lasertech) was used for scribing of the samples. Both devices, the laser and translation unit, were integrated inside the laser facility of PVcomB. The laser was operated at 50 kHz and maximum 2 W of average power. The pulse-to-pulse energy stability was ~1.5 %; the pulse duration was 35 ns. The patterning beam was sent through a multi-lens optical objective of 163 mm focal length. With the 3σ

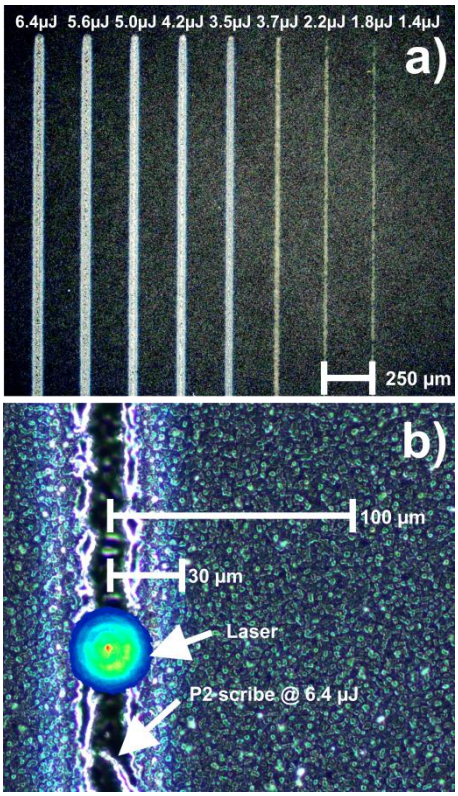

Figure 1. a) Optical microscope image of P2 scribe pattern obtained by scribing of CIGS samples at different pulse energies. b) Intensity profile of the scribing beam at 6.4 µJ with respect to the laser trench scribed by the same energy.

beam diameter of 30 µm in focus the beam was free from measurable astigmatism and had a Rayleigh length of~0.6 mm. It was characterized by a nearly Gaussian intensity profile (Figure 1b) and a 98% beam overlap related to the diameter was chosen. The scribing velocity was 20 mm/s. Nine discrete values of laser pulse energies, namely, 1.4 µJ, 1.8 µJ, 2,2 µJ, 2.7 µJ, 3.5 µJ, 4.2 µJ, 5.0 µJ, 5.6 µJ and 6.4 µJ were chosen to investigate thin-film CIGS degradation. They covered a full range of the process window used for phase transformation scribing and corresponded to an energy fluence range spanning from 0.25 $J \cdot cm^{-2}$ to 1 $J \cdot cm^{-2}$.

2.3 Characterization of Laser Affected Zone

The effect of laser illumination on CIGS was investigated systematically as a function of pulse energy and, as shown in Figure 2, as a function of distance from P2 scribes, which was measured perpendicularly to the laser trench. This general arrangement was applied to all types of investigations presented in the following part. A few complementary techniques were used to gain information about the properties of CIGS. Optical (Carl Zeiss AxioScope A1) and SEM microscopes (Hitachi S4100) were used to examine morphological changes, while stoichiometric changes among Zn, O, Cu, In, Ga, and Mo were investigated by means of the EDX. The acceleration energy of the electrons was 15 keV allowing for complete vertical penetration of CIGS (1.6 µm) on one side and effective excitation of K- and L-α lines on the other side. The spatial resolution of EDX measurements was ~1 µm, comparable to the size of individual CIGS grains. The surfaces of the samples were chemically prepared before

this type of measurements by etching off the TCO in diluted HCl solution. A triple Raman spectrometer (S&I TriVista, spectral resolution 0.6 cm^{-1}) was used for registering Raman spectra, subsequent to their excitation by the continuous wave (CW) 514 nm laser. Its power was set safely below the threshold of optical decomposition of CIGS to a sub mW level [15]. An optical microscope objective delivered the beam to the sample and collected at the same time the backscattered light. The laser spot obtained in this way had a diameter of 1 µm. The beam was moved above the surface of CIGS in 10 µm discrete steps to avoid convolution. The energetic structure of CIGS after P2 scribing was investigated by PL, excited by a CW laser at λ=532 nm. This wavelength was spectrally close to the one used for Raman excitation. The vertical penetration depths of light were thus comparable, but since a diameter of the PL beam was relatively large, i.e. approximately 20 µm, and the increment between laser spots only 10 µm, some beam overlap could not be avoided. We note that this effect was not further corrected. The wavelength resolution of the spectra was 0.5 nm. They were measured by low intensity of the laser of 3 µW. The setup used for PL measurements is schematically depicted in Figure 2.

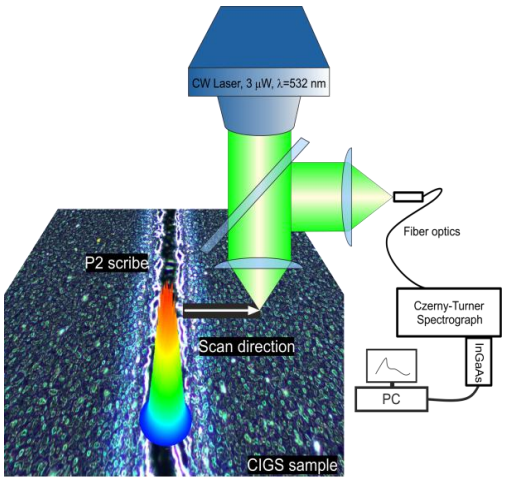

Figure 2. PL measurement setup.

3 Results

3.1 Optical and Electron Microscopy

No visual modification of probes could be found on their surfaces after the irradiation with laser pulses of 1.4 µJ energy. First changes begin to appear above 1.8 µJ, however, in this case an alteration of the surface takes place in the central part of the beam and is present only in TCO. A distinctive wide pale stripe develops at a pulse energy of 3.5 µJ. This stripe is shown in Figure 3a. At higher energies, the P2 scribes cause an opening of CIGS followed by melting and lateral displacement of material towards the edges of the beam. A distinguishable, rail-like structure is formed along the laser trench which can be easily observed under an optical or SEM microscope (Figure 3 b,d-e). We found that the rail-like structures create an interconnection between TCO and Mo, giving rise to a current flow through the P2 scribes [12]. Although the affected zone situated next to the melted

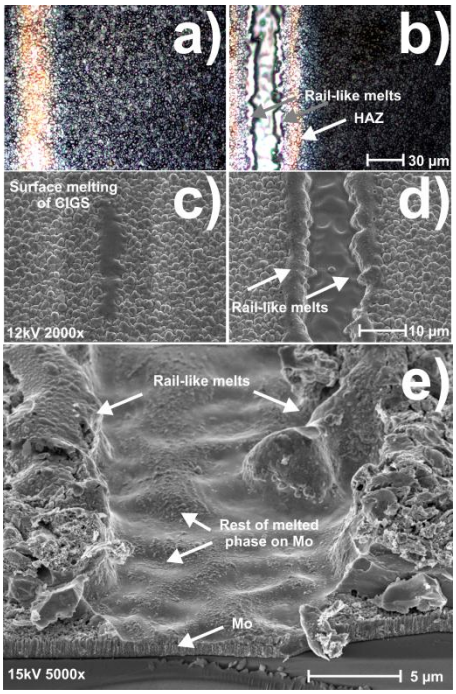

Figure 3. OM a-b) and SEM c-e) images of scribed CIGS samples. The energy of P2 laser pulse was 3.5 µJ and 6.4 µJ, respectively, for figures a,c) and c-e)

phase is very similar to this observed by lower pulse energies, its width exceeds by far the diameter of the incident laser beam, as indicated already in Figure 1b. Beyond the pale zone the absorber does not show any visible change or alteration. It has more or less constant dark grey color, so it is possible to use the optically changed area as an indicator of the heat affected zone (HAZ) [16]. As shown in many works the properties of CIGS are strongly affected within the HAZ leading to a change of its visual properties. The range of the HAZ can estimated by means of the thermal diffusion theory and the thermal diffusion length:

$$l_D = 2\sqrt{D \cdot \tau}\,. \qquad (1)$$

In the formula above l_D and D represent, respectively, the thermal diffusion length defining a distance of heat propagation in material during the time τ, and the heat diffusion coefficient. With τ =35 ns corresponding to duration of laser pulse used in our experiment and D=2.2×10^{-6} m^2/s [17] the l_D≅0.6 µm. It is approximately two orders of magnitude less than the measured range of visually changed CIGS, indicating that the laser pulse duration does not represent a good estimation the characteristic heat propagation time. More reliable results are obtained when assuming that thermal relaxation of CIGS is much slower than the laser pulse duration and persist over a time period corresponding to the laser repetition rate. By using a beam overlap of 98% and consecutive irradiation of the probe at 50 kHz over the traveled length of 1σ beam diameter (10 µm), we can calculate that l_D≅50 µm. The heat diffusion length estimated in this way is less than a factor of two different from the measured HAZ. This suggests that the energy concentrated in approximately one beam diameter contributes effectively to the thermal degeneration of CIGS represented by size of the visually changed zone. Interestingly, the 1σ beam diameter correlates well with the opening zone in CIGS, shown in Figures 3b,d-e. This

indicates that laser driven melting and thermal processes are likely to be related. A further analysis of scribes under SEM provides more detailed information on the surface morphology. It gives evidence of surface melting of CIGS at pulse energies of 3.5 µJ (Figure 3c), its partial opening by 4.47 µJ [18] and removal and dislocation of melted material at higher energies (Figure 3d-e), which was also observed under the optical microscope. Some remaining of the melted phase has also been found at the bottom of the opening of the scribe what is clearly indicated on a magnified SEM image from the Figure 3e).

3.2 Electron Dispersive X-Ray Spectroscopy

The EDX measurements have shown similar characteristics of the laser effect, namely, an increase of Zn, O, Ga and Cu concentration in the melted zone and evaporation of In from the melted zone and its vicinity for all applied laser pulse energies above 3.5 µJ. As shown in Figure 4a-b, this general tendency was much better pronounced at higher pulse energies. The absence of In can be well understood in terms of its low melting temperature (429.75 K) and low vaporization latent heat (231.8 kJ/mol), as compared to the other elements [12]. The accumulation of Cu in front of the other atoms in the melted zone (Figure 4b) proves very effective diffusion of this element in CIGS, which was observed previously by other groups [19]. The compositional changes in CIGS are only found inside the visually changed zone, up

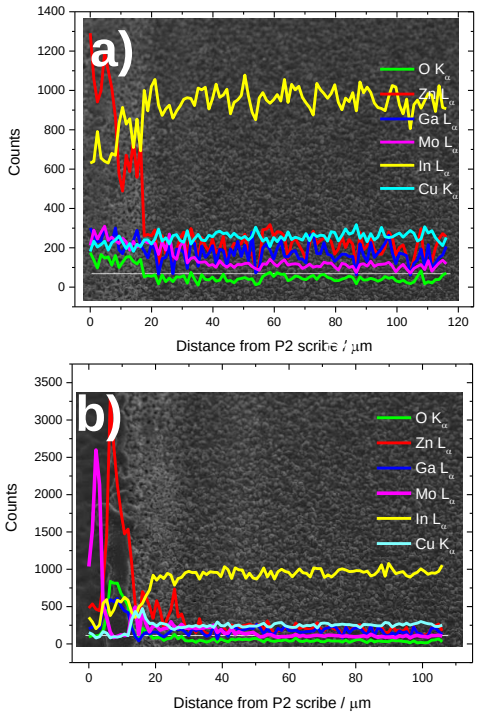

Figure 4. EDX analysis in direction perpendicular to the scribe across the opening , melted, heat affected and not affected zones. a) P2 scribe energy 3.5 µJ and b) 6.4 µJ.

to ~30 µm away from the scribes produced at 6.4 µJ pulse energy. They do not explain obvious differences in registered Raman and PL signals that, as we show below, were observed even 100 µm from the P2 scribes. We present more extensive, quantitative analysis of EDX data in [12].

3.3 Raman Spectroscopy

Raman spectroscopy is a versatile spectroscopic method, which allows to detect structural changes in thin-film CIGS [20,21] and we used this technique to indicate any structural changes caused by P2 laser irradiation. While the fundamental Se vibration mode A_1 (173 cm^{-1}) and a weak In-Se stretching mode B_2,E (213 cm^{-1}) provide information on crystallographic quality of CIGS, the fundamental 1 LO mode (~300 cm^{-1}) can be used to detect disorder or changes in the CdS buffer layer. The strongest E_2 Raman mode of ZnO at 434 cm^{-1} was outside of the available spectral range and could not be registered. The results shown in this chapter apply to P2 scribing laser irradiation at 6.4 µJ energy. In Figure 5a the Raman spectra obtained inside the visually

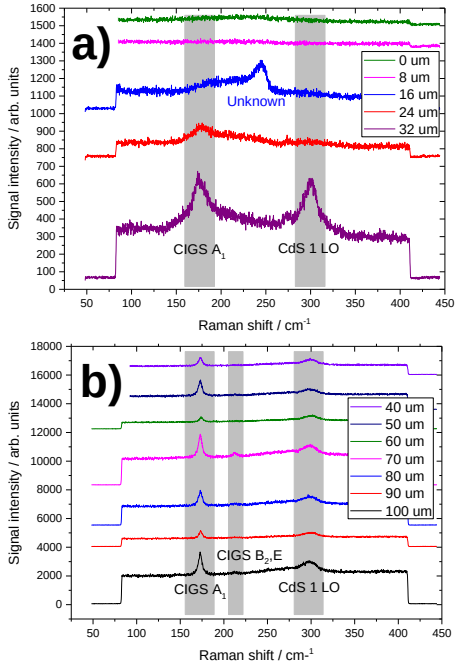

Figure 5. Raman signals as measured for the P2 scribe at 6.4 µJ energy.

changed zone up to 32 µm from the P2 scribe are shown, while in Figure 5b their evolution for distances from 40 µm to 100 µm are displayed. Since the Raman response from the bottom of the scribe (0 µm-8 µm) was zero, we can claim complete decomposition of the solar cell material in the middle of the scribe. The broad feature between 150 cm^{-1} and 250 cm^{-1} corresponding to a melted zone at 16 µm reveals a distinctive peak near 250 cm^{-1} which, however, could not be ascribed to any of the functional layers. It may be a result of some phase transition taking place during thermal cooling of the melted material. The first occurring signatures of CIGS and CdS registered, respectively, at 24 µm and 32 µm indicate preservation of the natural layer order, however, strong broadening of peaks indicates poor crystallinity. The range of structural changes in CIGS and CdS correspond well to the range of previously determined HAZ suggesting thermal decomposition of the crystallographic structure. We found that the intensity of the A1 (CIGS) and 1LO (CdS) peaks increases with a distance from the P2 scribes, even if this growth is strongly biased by signal fluctuations resulting most likely from the quality of individual crystal grains (Figure 6). Such behavior might indicate continuous

growth of CIGS mono-crystals, however, we found no evidence for such growth in SEM or OM images. The signal increase could have been also caused by increasing fraction of a highly crystalline phase within mono-crystals, but we have no direct evidence of such effect, either. A good crystallinity of CIGS far away from the P2 scribe was further confirmed by the presence of a weak B_2,E peak at distances greater than 60 µm. It is known that this peak indicates good binding of In and Se atoms in the lattice structure and will disappear by substantial vacancies of these elements [21].

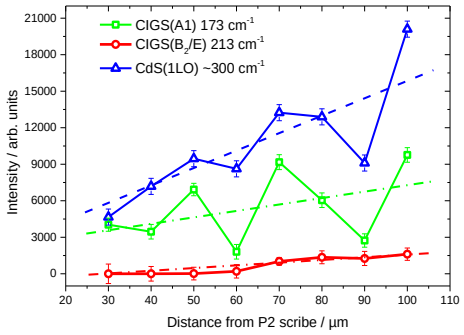

Figure 6. Evolution of Raman peaks intensities of the CIGS A1 and B_2,E modes and CdS 1LO mode.

3.4 Photoluminescence Spectroscopy

In order to evaluate changes of a band structure in CIGS the PL emission spectroscopy was used. Although this technique is often believed to provide information on the bandgap energy [23], we note that under the irradiation of semiconductors by light the position of the maximum in PL spectra does not represent the energy of the bandgap, but rater the quasi-Fermi level splitting, $\Delta\mu$, i. e. the difference between Fermi levels of electrons and holes, respectively, in conduction and valence bands [24]. In spite of it, the quasi-Fermi level splitting is a convenient parameter to describe the spectral distribution of PL, which is given by the equation:

$$\Phi_L(E_{ph}) = a(E_{ph})\frac{(E_{ph})^2}{4\pi^2\hbar^3c^3}\times \left[\exp\left(\frac{E_{ph}-\Delta\mu}{kT}\right)-1\right]^{-1}. \quad (2)$$

The equation above represents the generalized Planck's law with symbols denoting: the flux of emitted photons per solid angle and energy unit- Φ_L, the energy of emitted photons- E_{ph}, absorptivity of the probe- a, the Dirac constant- $\hbar$, the velocity of light in vacuum- c, the Boltzmann constant k, and the temperature T in Kelvin [25,26]. Despite different physical meaning, we will assimilate the nomenclature of *Malaquias et al.* [23] describing the position of the maximum in PL spectra as the bandgap energy. A fairly good impression of CIGS bandgap energy change is obtained when plotting the PL spectra as a function of distance from the P2 scribes. The curves in Figure 8a indicate the outcome of such procedure. Two characteristic observations can be made in this case, namely, that the amplitude of the PL signal decreases along with the position form the P2 scribe and that bandgap shifts towards lower energies. The first of the two mentioned features could also be observed in the Raman measurements (Figure 7b) and since the vertical penetration of radiation was comparable due to similar excitation wavelengths (514 nm vs. 532 nm) we can claim good correspondence of Raman and PL results. Figure 8b shows the effect of the bandgap shift. The bandgap energy, E_G, indicated above each of the curves was derived from the position of the maximum

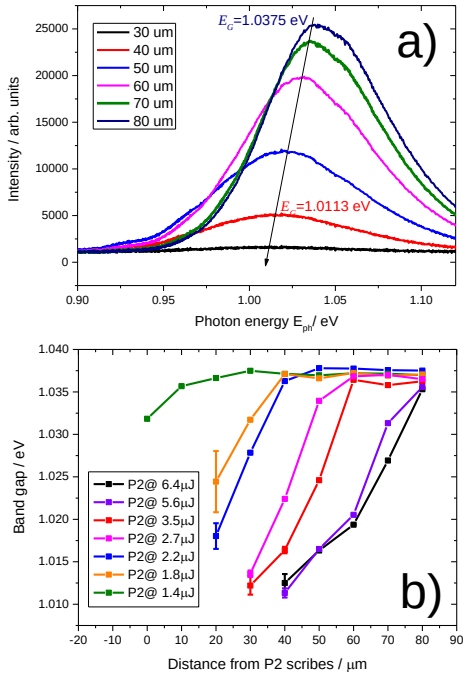

Figure 7. Investigation of the P2 scribe effect on bandgab enery. a) Raw PL signals of decreasing amplitude for P2 scribe at 5.6 µJ energy. b) Bandgap shift effet as function of P2 pulse energy and distance from P2 scribes..

of the fitted Gaussian curves. The inaccuracy of this procedure was in general in the order of 10^{-4} eV. The E_G changes from approximately 1.0375 eV for unaffected CIGS down to 1.0113 eV close to the P2 scribes and higher laser pulse energies. We found that below this minimum CIGS rather decomposes as indicated by the lack of PL emission. The change of E_G in CIGS is typically explained in terms of the change of the Ga to Ga+In stiochiometric ratio x=Ga/(Ga+In) [27] in the CIGS structure. However, no variation of x can be confirmed by EDX measurements, showing a fairly constant value of this parameter over the whole range of distances outside the HAZ. A possible explanation of this clear discrepancy are the different penetration depths of optical and electron beams, which was for EDX in the micron range and, thus, corresponding more or less to the thickness of CIGS while for PL it was only 150 nm. By the presence of Ga gradients in CIGS [28] the effective Ga concentrations seen by each of the beams may not be comparable. On the other hand, the PL and Raman studies both showed successive degradation of CIGS reaching even 80-100 µm from the P2 scribes. As such they consistently confirm an efficient decomposition of the semiconductor far away from the visually change zone what can be considered as rather unexpected.

Summary and Conclusion

We have systematically investigated the laser affected zone near the P2 phase transformation laser scribes applied to complete thin-film CIGS solar cell stacks. By choosing the scribing parameters in a range of the process window for industrial implementations of P2 scribes, we were able to recognize the limits of feasible degradation of CIGS in production lines. We showed that the degree of CIGS decomposition depends critically on the distance from the P2 scribes and the laser pulse energy. At low energies only surface changes of the TCO take place, while at higher energies substantial dislocation and melting of material from all cell layers is possible. The rail-like ridges are formed in this case in which stiochiometric relations are strongly altered as compared to unaffected CIGS. The concentration of low latent heat elements decreases, while these of higher latent heat increases. A signature of re-crystallization in the melted phase, occurring most likely during thermal relaxation after laser irradiation was found by performing Raman measurements, however, no specific chemical compound could be ascribed to this re-crystallized phase. Beyond the melted ridges the area of visually changed material was observed. Using a diffusion theory we have estimated that these changes could are related to the heat affected zone (HAZ). However, since short ns pulse duration of the scribing laser gives rise to very narrow thermal diffusion lengths of approximately 0.6 µm, we believe that the observed 30 µm wide HAZ must have resulted from the cooperative effect of many laser pulses. The Raman and PL spectroscopy indicated degradation of CIGS structure as far as to 100 µm from scribes, i. e. far beyond the HAZ. In case of the Raman spectroscopy these changes were evidenced by successive growth of CIGS A1, E_2,B peaks along with the distance from P2 scribes and lack of the CIGS E_2,B peak in the spectra registered at distances less than 60 µm. The PL spectroscopy, on the other hand, proved systematic shift of the quasi-Fermi level splitting in CIGS up to 80 µm from scribes, which was accompanied by systematic decrease of the PL signals' amplitude towards the position of the scribe. Our measurements show that the range of laser processing by phase-transformation P2 scribes in thin-film CIGS may exceed by far the beam diameter or the HAZ. They provide valuable information on the condition of CIGS and its degradation. As such they can be used for finding the most favorable positions of P1 and P3 scribes with respect to the P2 scribe. This type of optimization is necessary for reduction of a "dead area" in solar cells and manufacturing of best performing thin-film CIGS solar cells.

Acknowledgements

This work was supported by the Federal Ministry of Education and Research (BMBF) and the state government of Berlin (SENBWF) in the frame work of the program “Spitzenforschung und Innovation in den Neuen Ländern” (grant no. 03IS2151C).

References

1 T. Repmann, H. P. Kurz, M. Tech, P. Bockstadt, M. Oertel, D. Walter, D. Soeryanto, C. Jahn, J. Müller, and K. Orgassa, "Laser Processing, Module Manufacturing, CIGS, High-Efficiency," in *EU PVSEC Proceedings* (2013), pp. 2114 – 2117.

2. S. A. Pethe, M. J. Mendoza, A. Kaul, and N. G. Dhere, "Mechanical scribing as a quality and reliability analysis tool for CIGSeS thin film solar cells," 74120M–74120M (2009).

3. R. Murison, C. Dunsky, M. Rekow, C. Dinkel, J. Pern, L. Mansfield, T. Panarello, and S. Nikumb, "CIGS P1, P2, and P3 laser scribing with an innovative fiber laser," in *2010 35th IEEE Photovoltaic Specialists Conference (PVSC)* (2010), pp. 000179 –000184.

4. F. J. Pern, L. Mansfield, S. Glynn, B. To, C. DeHart, S. Nikumb, C. Dinkel, M. Rekow, R. Murison, T. Panarello, and C. Dunsky, "All-laser scribing for thin-film CuInGaSe2 solar cells," in *2010 35th IEEE Photovoltaic Specialists Conference (PVSC)* (2010), pp. 003479–003484.

5. A. Burn, M. Muralt, S. Pilz, V. Romano, R. Witte, B. Frei, S. Buecheler, S. Nishiwaki, and L. Krainer, "All Fiber Laser Scribing of Cu(In,Ga)Se2 Thin-Film Solar Modules," Physics Procedia **41**, 713–722 (2013).

6. . Burn, V. Romano, M. Muralt, R. Witte, B. Frei, S. Bücheler, and S. Nishiwaki, "Selective ablation of thin films in latest generation CIGS solar cells with picosecond pulses," in (2012), Vol. 8243, pp. 824318–824318–17.

7. G. Heise, A. Heiss, C. Hellwig, T. Kuznicki, H. Vogt, J. Palm, and H. P. Huber, "Optimization of picosecond laser structuring for the monolithic serial interconnection of CIS solar cells," Prog. Photovolt: Res. Appl. **21**, 681–692 (2013).

8. P.-O. Westin, U. Zimmermann, and M. Edoff, "Laser patterning of P2 interconnect via in thin-film CIGS PV modules," Solar Energy Materials and Solar Cells **92**, 1230–1235 (2008).

9. B. Stegemann, F. Fink, H. Endert, M. Schüle, C. Schultz, V. Quaschning, J. Niederhofer, and H.-U. Pahl, "Novel concept for laser patterning of thin film solar cells," Laser Technik Journal **9**, 25–29 (2012).

10. P.-O. Westin and M. Edoff, "Materials analysis of laser treated CIGS," in *23rd European Photovoltaic Solar Energy Conference : Proceedings of the International Conference Held in Valencia, Spain, 1-5 September 2008* (WIP-Renewable Energies, 2008), pp. 2558–2561.

11. P.-O. Westin, J. T. Wätjen, U. Zimmermann, and M. Edoff, "Microanalysis of laser micro-welded interconnections in CIGS PV modules," Solar Energy Materials and Solar Cells **98**, 172–178 (2012).

12. See our poster 3DV.1.56, "Laser-induced phase-transformation of CIGSe for monolithic interconnection: Analysis of the material properties".

13. M. Ruckh, J. Kessler, T. A. Oberacker, and H. W. Schock, "Thermal Decomposition of Ternary Chalcopyrite Thin Films," Jpn. J. Appl. Phys. **32**, 65 (1993).
14. B. Rau, F. Felice, N. Papathanasiou, C. Schultz, B. Stannowski, B. Szyzska, and R. Schlatmann, "Baseline meets innovation: Technology transfer for high-efficiency thin-film Si and CIGS modules at PVcomB," Photovoltaics International **17**, 99–106 (2012).
15. S. Prucnal, F. Jiao, D. Reichel, K. Zhao, S. Cornelius, M. Turek, K. Pyszniak, A. Drozdziel, W. Skorupa, M. Helm, and S. Zhou, "Influence of Flash Lamp Annealing on the Optical Properties of CIGS Layer," Acta Physica Polonica A **125**, 1404–1408 (2014).
16. A. Luft, U. Franz, L. Emsermann, and J. Kaspar, "A study of thermal and mechanical effects on materials induced by pulsed laser drilling," Appl. Phys. A **63**, 93–101 (1996).
17. A. . Compaan, I. Matulionis, and S. Nakade, "Laser scribing of polycrystalline thin films," Optics and Lasers in Engineering **34**, 15–45 (2000).
18. See our poster 3DV.1.55, "Investigation of CIGS thin film degradation under P2 scribe laser illumination".
19. K. Gartsman, L. Chernyak, V. Lyahovitskaya, D. Cahen, V. Didik, V. Kozlovsky, R. Malkovich, E. Skoryatina, and V. Usacheva, "Direct evidence for diffusion and electromigration of Cu in CuInSe2," Journal of Applied Physics **82**, 4282–4285 (1997).
20. Y. Yan, S. Li, Y. Ou, Y. Ji, C. Yan, L. Liu, Z. Yu, and Y. Zhao, "Structure and properties of CIGS films based on one-stage RF-sputtering process at low substrate temperature," J. Mod. Transport. **22**, 37–44 (2014).
21. J. Liu, D.-M. Zhuang, M.-J. Cao, C.-Y. Wang, M. Xie, and X.-L. Li, "Preparation and Characterization of $Cu(In,Ga)Se_2$ Thin Films by Selenization of $Cu_{0.8}Ga_{0.2}$ and In_2Se_3 Precursor Films," International Journal of Photoenergy **2012**, (2012).
22. X. Chuan-Ming, S. Yun, L. Feng-Yan, Z. Li, X. Yu-Ming, H. Qing, and L. Hong-Tu, "Composition-induced structural modifications in the quaternary CuIn1−xGaxSe2 thin films: bond properties versus Ga content," Chinese Phys. **16**, 788 (2007).
23. J. C. Malaquias, D. Regesch, P. J. Dale, and M. Steichen, "Tuning the gallium content of metal precursors for Cu(In,Ga)Se2 thin film solar cells by electrodeposition from a deep eutectic solvent," Phys. Chem. Chem. Phys. **16**, 2561–2567 (2014).
24. B. E. Pieters, T. Kirchartz, T. Merdzhanova, and R. Carius, "Modeling of photoluminescence spectra and quasi-Fermi level splitting in μc-Si:H solar cells," Solar Energy Materials and Solar Cells **94**, 1851–1854 (2010).
25. P. Wurfel, "The chemical potential of radiation," J. Phys. C: Solid State Phys. **15**, 3967 (1982).
26. A. Delamarre, L. Lombez, and J.-F. Guillemoles, "Contactless mapping of saturation currents of solar cells by photoluminescence," Applied Physics Letters **100**, 131108 (2012).
27. C. A. Durante Rincón, E. Hernández, M. I. Alonso, M. Garriga, S. M. Wasim, C. Rincón, and M. León, "Optical transitions near the band edge in bulk CuInxGa1−xSe2 from ellipsometric measurements," Materials Chemistry and Physics **70**, 300–304 (2001).
28. H. Mönig, C. A. Kaufmann, C.-H. Fischer, A. Grimm, R. Caballero, B. Johnson, A. Eicke, M. C. Lux-Steiner, and I. Lauermann, "Gallium gradients in chalcopyrite thin films: Depth profile analyses of films grown at different temperatures," Journal of Applied Physics **110**, 093509 (2011).